JASA ARTICLE

Coupled vibro-acoustic modeling of a dielectric elastomer loudspeaker

Emil Garnell,[a] Olivier Doaré,[b] and Corinne Rouby
IMSIA, CNRS, ENSTA Paris, EDF, CEA, Institut Polytechnique de Paris, France

ABSTRACT:
Dielectric elastomer membranes are soft electro-active materials capable of large deformations. When inflated over a cavity, the membrane radiates sound and can therefore be used as a loudspeaker. This type of device has been studied both experimentally and numerically. However, most studies on the dynamics of dielectric elastomer membranes either focus on the very low frequency behavior to analyse viscosity effects for example, or try to maximise the overall radiated sound pressure level. Here the mid-frequency range is analysed in detail, by setting up a fully coupled finite element model of an inflated dielectric elastomer membrane. Electrostatics, vibro-acoustics, free-field radiation, and pre-stressed linear dynamics are solved together, to find the fluid loaded resonance modes. The dynamics of the membrane and the sound radiation are then computed using this resonance mode basis. Perfectly matched layers are used to implement the Sommerfeld radiation boundary condition. The model is validated by a comparison with measurements of the pressure radiated by a prototype, and predicts accurately the radiated pressure and the directivity. This model should therefore help the development of optimized dielectric elastomer loudspeakers, with improved frequency responses and directivity. © *2020 Acoustical Society of America*.
https://doi.org/10.1121/10.0000930
(Received 22 November 2019; revised 11 February 2020; accepted 1 March 2020; published online 20 March 2020)
[Editor: Li Cheng] Pages: 1812–1821

I. INTRODUCTION

Dielectric elastomers are soft electro-active materials capable of large deformations. They are made of an elastomer membrane (typically silicone or acrylic), sandwiched between two compliant electrodes, usually made of conductive grease or carbon powder. When a high voltage is applied between the electrodes, the membrane thins down and expands in area by more than 100%.[1] This change in area can be exploited to generate a volume displacement, which will radiate sound. Several configurations have been suggested: the membrane can be inflated over a cavity,[3–6] mounted in a push–pull configuration,[7] or bent in a semi-cylindrical shape.[8]

The inflated configuration is very simple (see Fig. 1), and can be implemented in various settings as soon as a pressure differential is available. The rich dynamics of an inflated dielectric elastomer membrane have been studied experimentally by different research groups. The inflated configuration was first suggested by Heydt *et al.*[3,9] who studied the acoustical radiation, and demonstrated solutions to reduce distortion. Fox and Goulbourne[10,11] studied the dynamics of the membrane in more detail and examined the evolution of the first eigenfrequencies with respect to the main design parameters. On the acoustical point of view, the high frequency directivity of hemispherical and spherical inflated dielectric elastomer membranes was studied experimentally by Hosoya *et al.*[4,5] who demonstrated an omnidirectionnal radiation up to frequencies on the order of 16 kHz.

One of the limitations of this type of loudspeakers is the erratic frequency response at low and medium frequencies: it exhibits many drops and peaks generated by the membrane modes, and by the acoustic modes of the cavity over which the membrane is inflated. To improve the behavior in this frequency range, there is a need for a model taking into account all physics that govern the dynamics of the loudspeaker. Zhu *et al.*[12] derived a model describing the linear dynamics of a pre-inflated membrane, and compared the obtained eigenfrequencies to the experimental results of Fox and Goulbourne.[11] In a previous work,[6] we extended the linear model to take into account the interaction with the cavity on which the membrane is inflated, and to compute the forced response as well as the radiated pressure. Comparison with experiments showed relatively good accuracy. However, due to the small thickness of the membrane (typically around 100 μm), the surrounding air is comparatively heavy. Strong vibro-acoustic coupling therefore needs to be accounted for to yield an accurate prediction of the radiated pressure. What is more, there is, to the authors' knowledge, no theoretical or numerical study on the directivity of dielectric elastomer loudspeakers that could confirm Hosoya's results.[4,5]

In the present article, a coupled vibro-acoustic model of an inflated axisymmetric dielectric elastomer membrane is set up, and the radiated pressure is computed using modal methods. The system is damped, and open (exterior radiation), so complex resonance modes will be computed (in opposition to classical real un-damped modes[13]). The use of

[a]Electronic mail: emil.garnell@ensta-paris.fr, ORCID: 0000-0002-8555-1623.
[b]ORCID: 0000-0003-2219-9295.

https://doi.org/10.1121/10.0000930

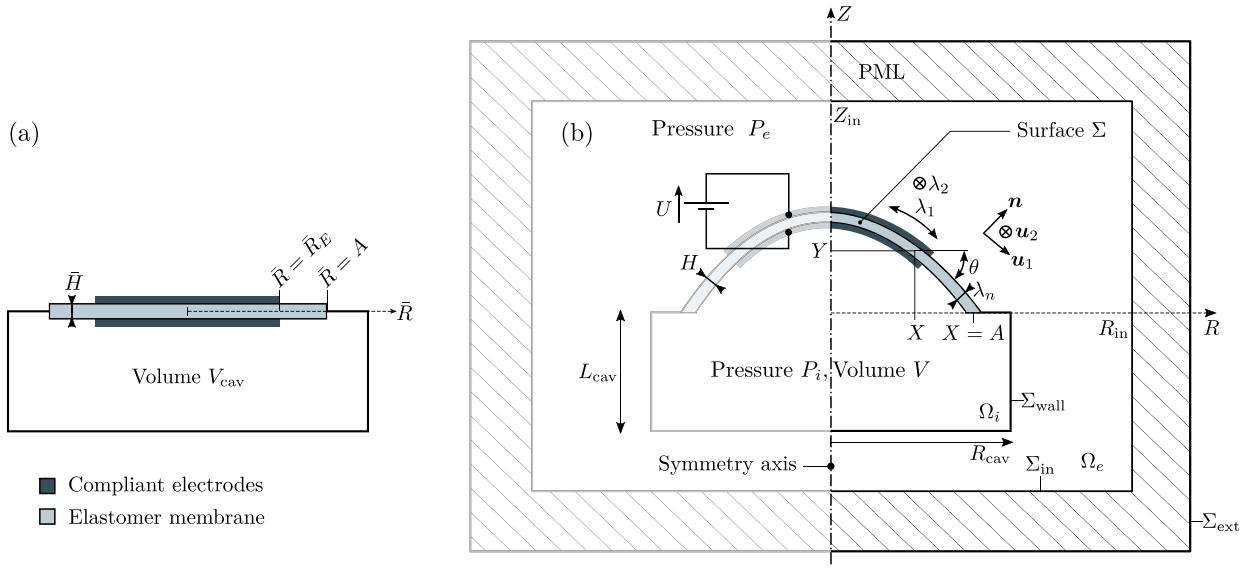

FIG. 1. (Color online) Schematics of the dielectric elastomer membrane. (a) Reference configuration. (b) Deformed configuration, and taking into account interior and exterior fluids. The model is axi-symmetric.

resonance modes as a reduced basis for the calculation of the forced response of open systems is an active field of research. Filippi *et al.*[13] derived an analytical modal expansion formula on the resonance mode basis, which is however, quite impractical. Marburg[14] studied the use of resonance modes as a basis to compute the radiated pressure of open systems in acoustics, and concluded that this method is particularly useful when only limited accuracy is required. There is substantial literature in the field of optics and photonics,[15,16] where nano-scale open light resonators have been investigated using resonance modes (also called quasi-normal modes). The coupling of finite element methods and perfectly matched layers (PMLs) appears to be one of the most efficient methods to compute resonance modes, and modal superposition is shown to work on such a reduced modal basis.

The present study serves two goals: improving the modelling and understanding of dielectric elastomer loudspeakers, and demonstrating the use of resonance modes to compute the pressure radiated in free field in a practical situation.

The paper is organized as follows: the studied problem is defined in Sec. II, the numerical method to solve the equations coupling electro-statics, mechanics, interior acoustics, and free-field radiation is described in Sec. III, and finally in Sec. IV, the numerical results are analysed and compared with measurements of the radiated pressure and directivity of a dielectric elastomer loudspeaker.

II. PROBLEM FORMULATION

This section largely builds upon previously published work by the authors,[6] where the dynamics and sound radiation of a dielectric elastomer membrane are studied. For the details of the derivation of the equations governing the membrane dynamics, the reader is referred to this publication. In the present article the strong coupling with acoustics is added compared to the previous work.

A. Description of the studied system

A circular membrane made of a soft isolating material, partially coated on both sides by compliant conductive electrodes, is considered. The membrane is inflated over a closed cavity, and a voltage applied between the electrodes vibrates the membrane which radiates sound in the surrounding air.

In the reference configuration, the membrane is flat and at rest [see Fig. 1(a)]. Its thickness is denoted as $\bar{H}$ and the radial coordinate as $\bar{R}$. The electrodes can be of any axisymmetrical shape, described by the function $\Gamma(\bar{R})$ which equals unity when electrodes are present at radius $\bar{R}$, and zero otherwise. In Fig. 1, $\Gamma(\bar{R}) = 1$ for $\bar{R} < \bar{R}_E$ and $\Gamma(\bar{R}) = 0$ for $\bar{R} > \bar{R}_E$. The membrane is clamped at its outer radius A over a cavity of initial volume V_{cav}.

Only axisymmetric deformations are studied in the present work. In the deformed configuration, the radial and axial positions of material points initially at radius $\bar{R}$ are denoted as X and Y, as indicated in Fig. 1(b). The thickness of the membrane is denoted as H, and its stretches along $\boldsymbol{u}_1$, $\boldsymbol{u}_2$, and $\boldsymbol{n}$ are denoted as $\lambda_1 = \sqrt{X' + Y'}$, $\lambda_2 = X/\bar{R}$, and λ_n. The prime ($'$) stands for the space derivative $\partial/\partial\bar{R}$. The membrane material is assumed to be incompressible so $\lambda_1\lambda_2\lambda_n = 1$.

During a first step, the membrane is inflated with the pressure P_{app}. The cavity is then closed: the amount of air in the cavity will be fixed during all the following steps.

In a second step a static voltage U_0 is applied between the electrodes. This voltage increases the area of the inflated membrane and thus increases the volume under the membrane to a value denoted as V_0, and decreases the pressure inside the cavity to a value denoted as P_0. The static equilibrium at the end of this second step will be referred to hereafter as the *static configuration*. In this configuration the radial and axial positions of the membrane are denoted as X_0 and Y_0, and its stretches λ_{10} and λ_{20}.

Finally, in a third step, an alternating voltage is superimposed to the static voltage:

$$U(T) = \sqrt{U_0^2 + W\cos(\Omega T)}, \quad \text{with } U_0^2 > W, \tag{1}$$

where $W\cos(\Omega T)$ is a dynamic excitation signal (in V^2). This form of the excitation cancels the non-linearity due to the quadratic dependence of the electrostatic stress on the electric field.[3] The linearized vibrations caused by the excitation W are studied, taking into account the couplings with interior and exterior acoustics. In order to obtain the linearized equations governing the system dynamics, small perturbations around the *static configuration*, written with a tilde, are introduced:

$$X = X_0 + \tilde{X}e^{i\Omega T}, \quad Y = Y_0 + \tilde{Y}e^{i\Omega T}. \tag{2}$$

B. Behavior of the dielectric elastomer

The coupling between the mechanics and electro-statics appears in the constitutive law relating the stress to the deformation, whose derivation is presented in detail by Edmiston and Steigmann *et al.*[17] or Zhu *et al.*[12] for example.

For the excitation signal given in Sec. II A, and using a Gent constitutive law for the elastomer,[18] the membrane principal stresses (along $\boldsymbol{u}_1$, $\boldsymbol{u}_2$) read:[6]

$$\sigma_1 = \frac{\mu(1+i\eta)J_m}{J_m - I_1 + 3}\left(\lambda_1^2 - \frac{1}{\lambda_1^2\lambda_2^2}\right) - \epsilon\Gamma\frac{U_0^2}{H^2} - \epsilon\Gamma\frac{W\cos(\Omega T)}{H^2}, \tag{3a}$$

$$\sigma_2 = \frac{\mu(1+i\eta)J_m}{J_m - I_1 + 3}\left(\lambda_2^2 - \frac{1}{\lambda_1^2\lambda_2^2}\right) - \epsilon\Gamma\frac{U_0^2}{H^2} - \epsilon\Gamma\frac{W\cos(\Omega T)}{H^2}, \tag{3b}$$

where μ is the shear modulus, J_m a parameter describing the stiffening of the material at large strains, and $\epsilon = \epsilon_0\epsilon_r$ the permittivity of the elastomer. The loss factor η is introduced to account for the dissipation. This simple damping model may be a simplification of the real damping phenomena that occur in dielectric elastomers.[19,20] However, in the present study the losses are small, so the numerical results are a little sensitive to the chosen damping model. More realistic damping may be taken into account by assigning a different modal loss factor to each membrane mode.

C. Membrane equilibrium equations

The membrane momentum balance equations projected along the axial and radial directions read:[6,12,21]

$$\rho_s(1+\Gamma\rho_{\text{ratio}})\frac{XH}{\cos\theta}\frac{\partial^2 X}{\partial T^2} = -\frac{\sigma_2 H}{\cos\theta} + (P_i - P_e)X\tan\theta + \frac{\partial}{\partial X}(\sigma_1 XH\cos\theta), \tag{4a}$$

$$\rho_s(1+\Gamma\rho_{\text{ratio}})\frac{XH}{\cos\theta}\frac{\partial^2 Y}{\partial T^2} = (P_i - P_e)X - \frac{\partial}{\partial X}(\sigma_1 XH\sin\theta), \tag{4b}$$

where ρ_s is the membrane density, ρ_{ratio} is the ratio of the electrode over the membrane mass per unit area, and the angle θ is defined in Fig. 1. The symmetry of the problem and the clamping of the membrane at the outer edge yields the following boundary conditions:

$$X(\bar{R}=0) = 0, \quad X(\bar{R}=A) = A, \quad Y'(\bar{R}=0) = 0, \quad Y(\bar{R}=A) = 0. \tag{5}$$

D. Acoustic equilibrium equations

The pressure difference between the inside and the outside of the cavity is small compared to the atmospheric pressure, so the fluid density ρ_f and the speed of sound C_f are assumed to be the same inside and outside.

The pressure field inside the cavity is split into a static part P_0, a uniform oscillating part P_u, and an acoustic part P_a:

$$P_i = P_0 + (P_u + P_a)e^{i\Omega T}. \tag{6}$$

The total dynamic pressure satisfies the Helmholtz equation, and the uniform pressure is proportional to the volume variation of the cavity. This yields the following system of governing equations:[22]

$$\Omega^2 P_a + \Omega^2 P_u + C_f^2\Delta P_a = 0, \tag{7a}$$

$$\int_{\Omega_i} P_a R\,dS = 0, \tag{7b}$$

$$P_u + C_f^2\frac{\rho_f}{V_0}2\pi\int_\Sigma \frac{1}{\lambda_{10}}(-Y_0'\tilde{X} + X_0'\tilde{Y})X_0\,dL = 0, \tag{7c}$$

where $dL = \lambda_{10}d\bar{R}$ is the element length of the membrane, and $dS = dRdZ$ the element surface of Ω_i and Ω_e.

The interior pressure satisfies Neumann boundary conditions: the normal velocity on the walls of the cavity is null, and the normal velocity equals the membrane normal velocity on the membrane Σ:

$$\nabla P_a \cdot \boldsymbol{n} = 0 \quad \text{on} \quad \Sigma_{\text{wall}}, \tag{8a}$$

$$\nabla P_a \cdot \boldsymbol{n} = \rho_f\Omega^2\frac{1}{\lambda_{10}}(-Y_0'\tilde{X} + X_0'\tilde{Y}) \quad \text{on} \quad \Sigma. \tag{8b}$$

The exterior pressure also obeys the Helmholtz equation:

$$\Omega^2 P_e + C_f^2\Delta P_e = 0, \tag{9}$$

and satisfies Neumann boundary conditions on the cavity walls and on the membrane:

https://doi.org/10.1121/10.0000930

$$\nabla P_e \cdot \boldsymbol{n} = 0 \text{ on } \Sigma_{\text{wall}}, \tag{10a}$$

$$\nabla P_e \cdot \boldsymbol{n} = -\rho_f \Omega^2 \frac{1}{\lambda_{10}} (-Y_0' \tilde{X} + X_0' \tilde{Y}) \text{ on } \Sigma, \tag{10b}$$

as well as a Sommerfeld radiation condition on the outer boundary Σ_{in}.

III. NUMERICAL SOLVING

The system of coupled Eqs. (3)–(10) presented in Sec. II is solved using finite elements. The weak forms of the equations need to be derived, and then discretized to obtain the mass and stiffness matrices. In this section, this process is described step by step.

A. Weak forms of the governing equations

First, in order to identify the independent parameters governing the problem, non-dimensional variables are defined, and written with lower case letters:

$$\begin{aligned}
&\bar{r} = \frac{\bar{R}}{A}, \quad r = \frac{R}{A}, \quad z = \frac{Z}{A},\\
&x = \frac{X}{A}, \quad y = \frac{Y}{A}, \quad t = \frac{C_s}{A} T, \quad \omega = \frac{A}{C_s} \Omega,\\
&p_a = \frac{A P_a}{\mu \bar{H}}, \quad p_e = \frac{A P_e}{\mu \bar{H}}, \quad p_0 = \frac{A P_0}{\mu \bar{H}}, \quad p_u = \frac{A P_u}{\mu \bar{H}},\\
&s_1 = \frac{\sigma_1}{\mu \lambda_1}, \quad s_2 = \frac{\sigma_2}{\mu \lambda_2}, \quad v_0 = \frac{V_0}{A^3},
\end{aligned} \tag{11}$$

where $C_s = \sqrt{\mu/\rho_s}$ is the speed of shear waves in the solid. In the following non-dimensional equations, the prime stands for space derivative $\partial/\partial \bar{r}$.

The use of the displacement potential instead of the acoustic pressure as state variable for the fluid will largely improve the convergence of the modal summation to compute the radiated pressure in Sec. III E. The displacement potentials are defined for interior and exterior acoustics as

$$p_a = \omega^2 q_a, \quad p_e = \omega^2 q_e. \tag{12}$$

Using the non-dimensional variables, the constitutive relations Eqs. (3) are re-written as

$$\begin{aligned}
s_1 = &\frac{(1+\mathrm{i}\eta) J_m}{J_m - I_1 + 3} \left(\lambda_1 - \frac{1}{\lambda_1^3 \lambda_2^2} \right) - u_0^2 \Gamma \lambda_1 \lambda_2^2\\
&- \frac{W \cos(\omega t) \epsilon}{\mu \bar{H}^2} \Gamma \lambda_1 \lambda_2^2,
\end{aligned} \tag{13a}$$

$$\begin{aligned}
s_2 = &\frac{(1+\mathrm{i}\eta) J_m}{J_m - I_1 + 3} \left(\lambda_2 - \frac{1}{\lambda_1^2 \lambda_2^3} \right) - u_0^2 \Gamma \lambda_1^2 \lambda_2\\
&- \frac{W \cos(\omega t) \epsilon}{\mu \bar{H}^2} \Gamma \lambda_1^2 \lambda_2,
\end{aligned} \tag{13b}$$

where $u_0 = U_0 \sqrt{\epsilon/\mu \bar{H}^2}$ is the non-dimensional static voltage. These relations are linearized around the *static configuration* when the dynamics are computed, to obtain the linear excitation caused by the alternating signal $W \cos(\omega t)$.

Multiplying Eq. (4) by test functions $\mathcal{X}$ and $\mathcal{Y}$, and integrating by part yields the following weak form of the membrane equilibrium equations:

$$\begin{aligned}
&\int_\Sigma \mathcal{Y}' \frac{\bar{r} s_1 y'}{\lambda_1^2} \mathrm{d}l + \int_\Sigma \mathcal{X}' \frac{\bar{r} s_1 x'}{\lambda_1^2} \mathrm{d}l + \int_\Sigma \frac{1}{\lambda_1} s_2 \mathcal{X} \mathrm{d}l\\
&\quad - \int_\Sigma \frac{1}{\lambda_1} (p_0 + p_u)(-y' \mathcal{X} + x' \mathcal{Y}) x \mathrm{d}l\\
&= - \int_\Sigma \frac{1}{\lambda_1} (1 + \Gamma \rho_{\text{ratio}}) \left(\mathcal{Y} \frac{\partial^2 y}{\partial t^2} + \mathcal{X} \frac{\partial^2 x}{\partial t^2} \right) \bar{r} \mathrm{d}l\\
&\quad - \int_\Sigma \frac{1}{\lambda_1} \frac{\partial^2}{\partial t^2} (q_a - q_e)(-y' \mathcal{X} + x' \mathcal{Y}) x \mathrm{d}l,\\
&\forall \mathcal{X}, \mathcal{Y}, \ |\mathcal{X}(\bar{r} = 1) = \mathcal{Y}(\bar{r} = 1) = 0.
\end{aligned} \tag{14}$$

To compute the linear dynamics, this weak form is then linearized around the *static configuration*.

Multiplying Eq. (7c) by a test scalar $\mathcal{P}_u$ yields the weak form of the equation governing the uniform pressure in the cavity:

$$\mathcal{P}_u p_u + \mathcal{P}_u \frac{m c^2}{v_0} 2\pi \int_\Sigma \frac{1}{\lambda_{10}} (-y_0' \tilde{x} + x_0' \tilde{y}) x_0 \mathrm{d}l = 0, \quad \forall \mathcal{P}_u, \tag{15}$$

where $c^2 = C_f^2/C_s^2$ is a non-dimensional parameter describing the relation between the speed of sound in the membrane and in the air, and $m = \rho_f A/\rho_s \bar{H}$ is a parameter describing how heavy the fluid is compared to the membrane.

Multiplying Eq. (7a) by a test function $\mathcal{Q}_a$, integrating by parts, taking into account the boundary conditions, and using a Lagrange multiplier κ_i to ensure the mean pressure constraint (7b) yields the weak form of the Helmholtz equation governing the interior pressure:

$$\begin{aligned}
&-\omega^2 \int_{\Omega_i} q_a \mathcal{Q}_a r \mathrm{d}s + c^2 \int_{\Omega_i} \nabla q_a \cdot \nabla \mathcal{Q}_a r \mathrm{d}s - \int_{\Omega_i} p_u \mathcal{Q}_a r \mathrm{d}s\\
&-mc^2 \int_\Sigma \frac{1}{\lambda_{10}} (-y_0' \tilde{x} + x_0' \tilde{y}) \mathcal{Q}_a x_0 \mathrm{d}l\\
&+\kappa_i \int_{\Omega_i} \mathcal{Q}_a r \mathrm{d}s + \mathcal{K}_i \int_{\Omega_i} q_a r \mathrm{d}s = 0, \quad \forall \mathcal{Q}_a, \forall \mathcal{K}_i.
\end{aligned} \tag{16}$$

The weak form of the Helmholtz equation governing exterior acoustics is obtained in a similar manner:

$$\begin{aligned}
&-\omega^2 \int_{\Omega_e} q_e \mathcal{Q}_e r \mathrm{d}s + c^2 \int_{\Omega_e} \nabla q_e \cdot \nabla \mathcal{Q}_e r \mathrm{d}s\\
&+mc^2 \int_\Sigma \frac{1}{\lambda_{10}} (-y_0' \tilde{x} + x_0' \tilde{y}) \mathcal{Q}_e x_0 \mathrm{d}l = 0, \quad \forall \mathcal{Q}_e.
\end{aligned} \tag{17}$$

Due to the Sommerfeld condition at the outer boundary of the exterior domain, a special treatment of this boundary has to be made. This is done in Sec. III B, where PMLs are derived to get a correct weak form for exterior acoustics.

B. Perfectly matched layers for acoustic radiation

PMLs are an efficient way to ensure reflection-free boundary conditions in a finite element calculation. They consist of an added absorbing layer placed around the outer boundary [here for $r > r_{\text{in}}$ and $|z| > z_{\text{in}}$, see Fig. 1(b)]. PMLs have first been suggested by Berenger[23] for calculations in the time domain, but they are well suited to frequency domain computations as well. Here axisymmetric PMLs are used, with the complex change of variables given by Colino and Monk.[24] A single change is made with respect to Collino and Monk's work: the frequency dependence of change of variable is removed so that frequency independent mass and stiffness matrices can be obtained. Thus, we define

$$\hat{r} = \begin{cases} r - \mathrm{i}\displaystyle\int_{r_{\text{in}}}^{r} \Theta_r(r)\mathrm{d}s & \text{for } r > r_{\text{in}} \\ r & \text{otherwise,} \end{cases} \tag{18a}$$

$$\hat{z} = \begin{cases} z - \mathrm{i}\displaystyle\int_{z_{\text{in}}}^{z} \Theta_z(z)\mathrm{d}s & \text{for } |z| > |z_{\text{in}}| \\ z & \text{otherwise,} \end{cases} \tag{18b}$$

where classical quadratic attenuation functions are chosen:

$$\Theta_r(r) = \Theta_0(r - r_{\text{in}})^2, \quad \Theta_z(z) = \Theta_0(z - z_{\text{in}})^2, \tag{19}$$

Θ_0 being an attenuation parameter that should be adjusted.

These changes of variables imply the following changes of the partial derivatives:

$$\frac{\partial}{\partial \hat{r}} = \frac{1}{\gamma_r(r)}\frac{\partial}{\partial r}, \quad \frac{\partial}{\partial \hat{z}} = \frac{1}{\gamma_z(z)}\frac{\partial}{\partial z}, \tag{20}$$

where the γ_i functions are defined as follows:

$$\gamma_r(r) = \begin{cases} 1 - \mathrm{i}\Theta_r(r) & \text{for } r > r_{\text{in}} \\ 1 & \text{otherwise,} \end{cases} \tag{21}$$

$$\gamma_z(z) = \begin{cases} 1 - \mathrm{i}\Theta_z(z) & \text{for } |z| > |z_{\text{in}}| \\ 1 & \text{otherwise.} \end{cases} \tag{22}$$

The changes of variables Eqs. (18) are inserted in the weak form governing exterior acoustics (17):

$$\begin{aligned} &-\omega^2 \int_{\Omega_e} q_e \mathcal{Q}_e \hat{r}\mathrm{d}s \\ &+c^2 \int_{\Omega_e} \left(\frac{\gamma_z}{\gamma_r}\frac{\partial q_e}{\partial r}\frac{\partial \mathcal{Q}_e}{\partial r} + \frac{\gamma_r}{\gamma_z}\frac{\partial q_e}{\partial z}\frac{\partial \mathcal{Q}_e}{\partial z} \right) \hat{r}\mathrm{d}s \\ &+mc^2 \int_{\Sigma} \frac{1}{\lambda_{10}} \left(-y_0'\tilde{x} + x_0'\tilde{y} \right) \mathcal{Q}_e x_0 \mathrm{d}l = 0, \quad \forall \mathcal{Q}_e. \end{aligned} \tag{23}$$

If the parameter Θ_0 of the PMLs is correctly chosen, the reflections of outgoing waves on the PMLs should be negligible in the frequency range of interest. This will be validated in Sec. IV A.

C. Discretization of the weak forms using finite elements

The weak forms derived in Secs. III A and III B are discretized using finite elements, implemented in the FreeFEM software.[25]

In the first step, only the membrane is considered, and the static inflation with the pressure P_{app} is computed. In the second step, the static voltage U_0 is added, and the new equilibrium is computed as well. For these two steps, the membrane is meshed in the reference configuration by 150 2D Lagrange P2 elements along the radius. The non-linear static equilibrium is computed by a Newton–Raphson method. At the end of this static calculation, $x_0(\bar{r})$, $y_0(\bar{r})$ and their derivatives, as well as p_0 and v_0 are known.

In the third step, the linear dynamics of the membrane around the *static configuration* are computed. The membrane and the interior and exterior fluids are meshed this time in the *static configuration*. Lagrange P2 elements are used in all domains. The meshed geometry is shown in Fig. 2. The number of elements along the radius of the membrane is chosen so that there are 12 elements per flexural wavelength at 5 kHz, and similarly the number of acoustic elements is chosen so that there are 12 elements per acoustic wavelength at 5 kHz. The pressure fluctuations close to the membrane are governed by the wavelength of the flexural waves in the membrane and not by the acoustic wavelength. Therefore, at the interface the size of the acoustic elements is the same as the size of the membrane elements.

The PML parameters (thickness, attenuation Θ_0, and distance from the membrane) have been adjusted on a numerical test case, consisting of a flat piston embedded in an infinite baffle. For this setup, the Rayleigh integral

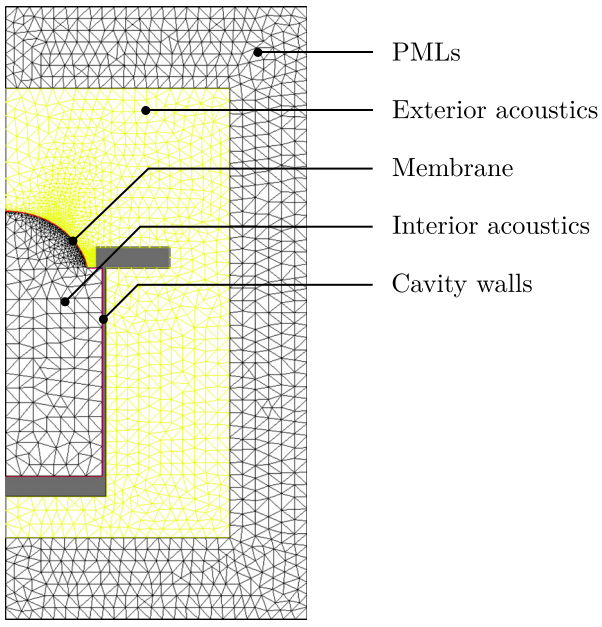

FIG. 2. (Color online) Mesh of the fully coupled model. The yellow area is the acoustical domain, the exterior black area is the PML, the interior black area is the interior fluid, and the membrane mesh is too thin to be visible on this picture. The grey area corresponds to the walls of the cavity.

https://doi.org/10.1121/10.0000930

provides an exact solution for the radiated pressure. The code for this test case and further details are available as supplementary material.[2]

D. Assembly of coupled mass and stiffness matrices

To couple the different physics (electrostatics, mechanics, and acoustics), the total stiffness and mass finite element matrices are assembled as follows:

$$\boldsymbol{M}_{\text{tot}} = \begin{bmatrix} M_a & 0 & 0 & 0 & 0 \\ 0 & 0 & 0 & 0 & 0 \\ 0 & 0 & 0 & 0 & 0 \\ 0 & 0 & 0 & M_e & 0 \\ M_s^a & 0 & 0 & M_s^e & M_s \end{bmatrix}, \tag{24}$$

$$\boldsymbol{K}_{\text{tot}} = \begin{bmatrix} K_a & K_a^\kappa & K_a^u & 0 & K_a^s \\ K_\kappa^a & 0 & 0 & 0 & 0 \\ 0 & 0 & K_u & 0 & K_u^s \\ 0 & 0 & 0 & K_e & K_e^s \\ 0 & 0 & K_s^u & 0 & K_s \end{bmatrix}, \tag{25}$$

where the different sub-matrices are defined by the weak forms derived in Secs. III A and III B. Equations (16) and (23) lead to the mass and stiffness matrix for interior and exterior acoustics M_a, K_a, M_e, and K_e; and Eq. (14) to the membrane matrices M_s and K_s. The matrix K_u is the stiffness added by the cavity, coming from Eq. (15); K_a^u is the coupling between the interior acoustic pressure and the uniform pressure from Eq. (16); K_a^κ and K_κ^a are the terms related to the Lagrange multiplier insuring the zero mean pressure for interior acoustics in Eq. (16). The remaining sub-matrices $M_s^a, M_s^e, K_a^s, K_u^s, K_e^s, K_s^u$ describe the coupling between acoustics and the membrane, and between the membrane and the cavity stiffness [defined by Eqs. (14)–(16) and (23)].

The total system reads:

$$(-\omega^2 \boldsymbol{M}_{\text{tot}} + \boldsymbol{K}_{\text{tot}})\boldsymbol{X}_{\text{tot}} = \boldsymbol{F}_{\text{tot}}, \tag{26}$$

where $\boldsymbol{X}_{\text{tot}} = [q_a, \kappa, p_u, q_e, [\tilde{x}, \tilde{y}]]^T$ and $\boldsymbol{F}_{\text{tot}} = [0, 0, 0, 0, \mathcal{F}]^T$. The force $\mathcal{F}$ is the electrostatic force applied on the membrane, due to the terms in W in Eqs. (13). The matrices $\boldsymbol{M}_{\text{tot}}$ and $\boldsymbol{K}_{\text{tot}}$ are both frequency independent.

E. Forced response

A first method to solve the system (26) is to use a direct approach: the system is inverted for all frequencies of interest,

$$\boldsymbol{X}_{\text{tot}} = (-\omega^2 \boldsymbol{M}_{\text{tot}} + \boldsymbol{K}_{\text{tot}})^{-1} \boldsymbol{F}_{\text{tot}}. \tag{27}$$

This method, later referred to as the *Finite Element Method (FEM)*, may be time consuming if many frequency bins are required and provides poor physical interpretation of the results.

A second option is to use a modal approach, which provides a clearer physical interpretation of the obtained frequency response, and is much more efficient to compute several frequency response functions of the same system but with various excitation forces. Indeed, the matrices have been built in order to be frequency independent (frequency-independent PMLs, structural damping). As a consequence, a linear eigenvalue problem is obtained. Standard eigenvalue solvers are therefore used to compute the modes of the homogeneous system (26) with $\boldsymbol{F}_{\text{tot}} = 0$.

In the present case, the mass and stiffness matrices are not symmetric so left and right eigenvectors (Ψ_n^L and Ψ_n^R) need to be computed:

$$\boldsymbol{\Psi}_n^L(-\omega_n^2 \boldsymbol{M}_{\text{tot}} + \boldsymbol{K}_{\text{tot}}) = 0, \tag{28}$$

$$(-\omega_n^2 \boldsymbol{M}_{\text{tot}} + \boldsymbol{K}_{\text{tot}})\boldsymbol{\Psi}_n^R = 0. \tag{29}$$

We recall that the resonance frequencies ω_n are complex due to the losses in the PMLs and to the structural damping η. If all eigenvalues are of order 1 (which has been checked here), the following bi-orthogonality relations hold:

$$\boldsymbol{\Psi}^L \boldsymbol{M}_{\text{tot}} \boldsymbol{\Psi}^R = \mathbf{diag}(m_n), \quad \boldsymbol{\Psi}^L \boldsymbol{K}_{\text{tot}} \boldsymbol{\Psi}^R = \mathbf{diag}(k_n), \tag{30}$$

where m_n and k_n are the modal mass and stiffness of mode n, and $\boldsymbol{\Psi}^L$ and $\boldsymbol{\Psi}^R$ are the matrices containing the left and right modeshapes. The modal force is defined as $F_n = Y_n^L \boldsymbol{F}_{\text{tot}}$. The total displacement is projected onto the right modeshapes basis $\boldsymbol{X}_{\text{tot}} = \boldsymbol{\Psi}^R \boldsymbol{\alpha}$. Inserting this into Eq. (26), left-multiplying by $\boldsymbol{\Psi}^L$, and using the bi-orthogonality relations allows us to express the modal amplitudes as

$$\alpha_n(\omega) = \frac{F_n}{m_n(\omega_n^2 - \omega^2)}. \tag{31}$$

The displacement and the acoustic pressure are then known everywhere:

$$\tilde{x} = \sum_n \alpha_n(\omega)\Psi_{n,x}^R, \quad \tilde{y} = \sum_n \alpha_n(\omega)\Psi_{n,y}^R, \tag{32}$$

where $\boldsymbol{\Psi}_n^R$ has been split into parts containing the different types of degrees of freedom, $\Psi_{n,e}^R$ containing for example the exterior acoustics degrees of freedom. This method will be referred to as the *Modal* method. Due to the use of the displacement potential as the state variable for the fluid, the obtained pressure is proportional to the membrane acceleration, which is expected for acoustic radiation. If the pressure had been used instead as the state variable, the radiated pressure would have been proportional to the displacement, which would have led to poor convergence of the modal summation for the radiated pressure.

The *Modal* method works to compute the pressure in the near field, in the part of the acoustical domain that is meshed (see Fig. 2). If the far field pressure is needed, this near field solution is propagated using the Kirshoff–Helmholtz integral:

$$P_e(\boldsymbol{x}_r) = -\int_{\Sigma_{KH}} (P_e(\boldsymbol{x})\nabla G(\boldsymbol{x},\boldsymbol{x}_r)\cdot\boldsymbol{n}(\boldsymbol{x}) - \nabla P_e(\boldsymbol{x})\cdot\boldsymbol{n}(\boldsymbol{x})G(\boldsymbol{x},\boldsymbol{x}_r))\mathrm{d}S(\boldsymbol{x}), \quad (33)$$

where Σ_{KH} is a surface enclosing the loudspeaker [see Fig. 3(a)], $\boldsymbol{x}_r$ is the location of the receiver, $\boldsymbol{n}(\boldsymbol{x})$ is the outer normal to Σ_{KH}, and G is the free-field Green's function:

$$G(\boldsymbol{x},\boldsymbol{x}_r) = \frac{\mathrm{e}^{-\mathrm{i}||\boldsymbol{x}-\boldsymbol{x}_r||\Omega/C_f}}{4\pi||\boldsymbol{x}-\boldsymbol{x}_r||}. \quad (34)$$

The modal expansion of P_e (32) can be used in Eq. (34), and this method will be referred to as *Modal KH*.

F. Truncation of the modal basis

When the modes of a resonant system coupled to an exterior fluid are computed using PMLs, two types of modes will be obtained:[15] the resonant modes of the fluid loaded structure [referred to hereafter as *membrane modes*, see Fig. 3(a)], and a series of so-called *PML modes* [see Fig. 3(b)]. The *PML modes* arise from reflections inside the PMLs, so they will change both in frequency and in shape if the PML parameters (size, attenuation…) are changed. The two types of modes (*membrane* and *PML modes*) must be included in the modal summation to provide accurate reconstructions of the acoustic and structural responses. In the present study the modal basis is truncated by selecting all the modes that have an absolute value of their eigenfrequency below a given threshold. The threshold is chosen so that the modal solution is close enough to the direct calculation (*FEM*).

Different modal basis truncations have been suggested by Marburg[14] for example. However, in the present context, selecting the relevant modes according to the absolute value of their eigenfrequencies performs well. This requires us to run the costly direct calculation (*FEM*) one time. Yet, once the modes are computed and the modal truncation criterion is defined, calculating various frequency responses for various excitations can be performed quickly using the modal approach.

Both the structural and the acoustic response are dominated by *membrane modes* (see Fig. 8, where each peak correspond to a *membrane mode*) and it is interesting to study only these modes for the physical interpretation they provide.

The pressure in the *PML modes* is very large inside the PMLs and smaller in the physical part of the model [see Fig. 3(b)]. As the PML is largely damped, *PML modes* have a high modal loss factor. A damping criterion is thus used to distinguish *membrane modes* from *PML modes*. Figure 4 shows that there is a clear distinction in damping between *PML modes* and *membrane modes*, and that the chosen criterion is efficient in sorting out the different modes. As emphasized in Fig. 4, the damping value of 5% will be used in Sec. IV to distinguish between the two types of modes.

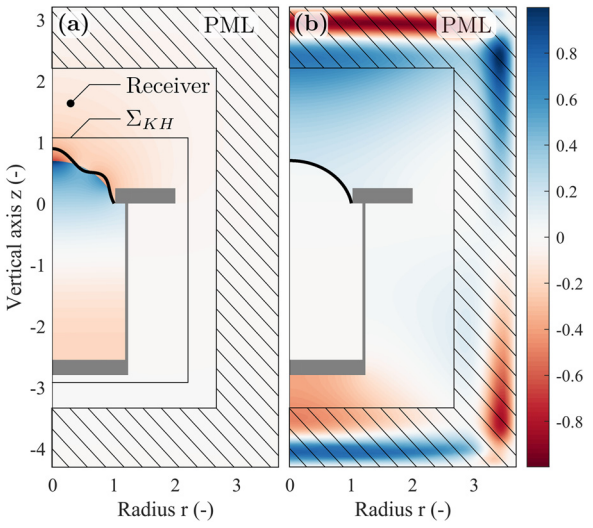

FIG. 3. (Color online) (a) Example of a *membrane mode*, and definition of the receiver location and integration surface for the Kirshoff Helmholtz integral. (b) Example of a *PML mode*, where the pressure in the PML layer is large. The color scale for the acoustic pressure is the same on both plots.

IV. RESULTS

In this section, the model is used to investigate fluid loading effects on the vibrations of a real membrane, on which experiments are also conducted. All numerical and experimental results presented in this paper are obtained with the dimensional and non-dimensional parameters given in Table I.

The frequency response functions are computed by three methods:

- *FEM*: the system (26) is solved for all frequencies of interest.
- *Modal*: the modal method described in Sec. III E is used to compute the near-field pressure. The first 250 computed modes (sorted by increasing absolute value of the resonance frequency) were all used in the modal expansion, including *PML modes*.
- *Modal KH*: the near-field pressure computed using the *Modal* method is propagated to the far-field using the Kirshoff–Helmholtz integral. The same modes are used as for the *Modal* method.

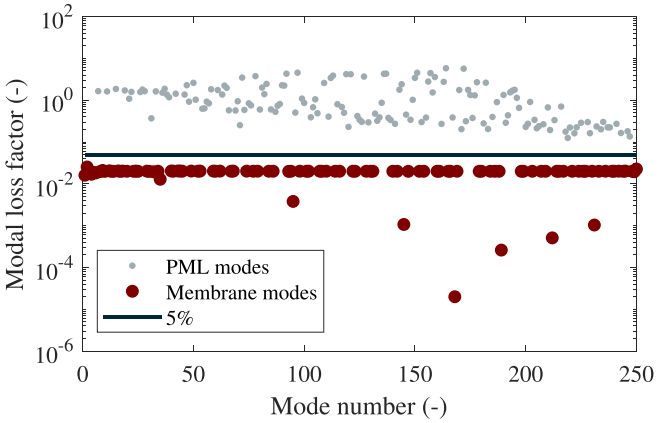

FIG. 4. (Color online) Computed modal loss factor of the first 250 modes. The structural loss factor η is set to 4%, so all modes with a damping higher than 5% are considered to be *PML modes*.

https://doi.org/10.1121/10.0000930

TABLE I. List of all experimental dimensional parameters (Dim.) and non-dimensional parameters (Non-dim.). These parameters are used in all experiments and numerical results presented in the present paper.

Dim.	Value	Non-dim.	Value
H_0	126 μm	—	—
V_{cav}	0.72L	$v_{cav} = V_{cav}/A^3$	11.2
$\bar{R}_E$	4 cm	$\bar{r}_E$	1
μ	2.0×10^5 Pa	—	—
P_{app}	800 Pa	p_{app}	1.27
ρ_s	1042 kgm^{-3}	—	—
J_m	1000	J_m	1000
U_0	1200 V	u_0^2	0.011
ρ_{elec}	0.09 kg m^{-2}	ρ_{ratio}	0.69
A	4 cm	—	—
W	2×10^5 V^2	—	—
ϵ_r	2.8	—	—
η	4%	η	4%
C_f	343 m s^{-2}	c^2	613
ρ_f	1.2 kg m^{-3}	m	0.37
L_{cav}	10.2 cm	$l_{cav} = L_{cav}/A^3$	2.55
R_{cav}	4.7 cm	$r_{cav} = R_{cav}/A^3$	1.18

A. Validation of the PML implementation and modal expansion

The near field pressure calculated using the *FEM*, *Modal*, and *Modal KH* methods is plotted in Fig. 5. The pressures calculated using the *Modal* and the *Modal KH* methods are equal. Figure 5 validates the use of the Kirshoff–Helmholtz integral to propagate the pressure. The *KH* integral assumes that there are no reflections outside of Σ_{KH}, this result also validates the PML implementation.

What is more, the modal expansion yields almost the same results as the *FEM* direct calculation. There is a slight deviation at high frequencies which is likely due to a too small number of modes used in the modal summation. Overall, Fig. 5 shows that the modal approach is efficient even for this exterior acoustic problem. The modal method has been tested with only the 75 *membrane modes* contained in the first 250 modes, and gives unsatisfactory results. This is consistent with the observations of Lalanne *et al.*,[15] where they notice that *PML modes* should be included to reach good accuracy.

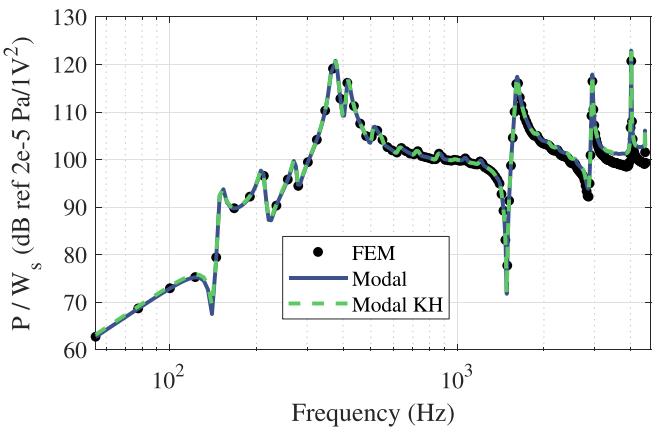

FIG. 5. (Color online) Comparison of the transfer functions between the pressure at the receiver's location for three different calculation methods: *FEM*, *Modal*, and *Modal KH*. The first 250 modes are used in the modal expansion (including *PML modes*).

B. Influence of the fluid loading on *membrane modes*

The influence of the fluid loading on the *membrane modes* is studied. The resonance frequencies are plotted in Fig. 6, in which the modes are ordered by ascending real part of their resonance frequency.

These figures show that the fluid loading has a strong impact on the membrane vibrations. The resonance frequencies are decreased by up to 15% when fluid loading is accounted for. This result points out an added mass effect.

C. Frequency response functions

A prototype is built (see Fig. 7), following the same process as Garnell *et al.*[6] The membrane is made of spin-coated Nusil CF19-2186 silicone. The thickness is measured by a laser displacement sensor, with an accuracy of 5 μm. The material parameters μ and J_m are adjusted on

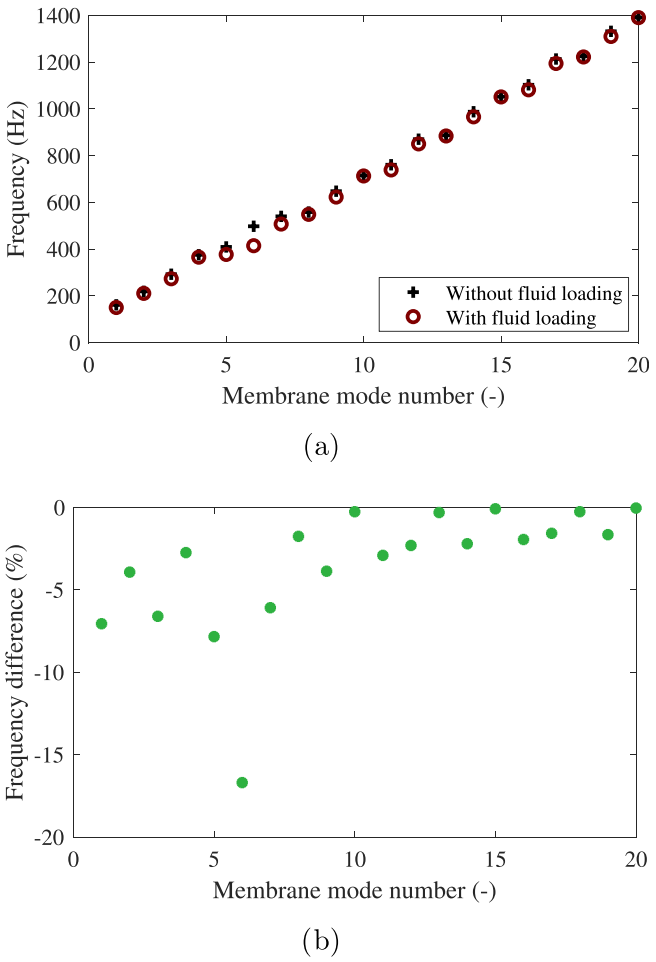

FIG. 6. (Color online) Influence of the fluid loading on the first 20 *membrane modes*. (a) First 20 *membrane mode* eigenfrequencies with and without taking into account heavy fluid effects. (b) Relative difference of the *membrane mode* eigenfrequencies due to the fluid loading effect.

FIG. 7. (Color online) Prototype of a dielectric elastomer loudspeaker, during radiation and directivity measurements in an anechoic chamber.

comparisons between the measured and calculated static deformation of the membrane without voltage.

The transfer function between the excitation signal W and the radiated acoustic pressure at 12 cm is measured in an anechoic chamber. This transfer function is also computed using the *modal KH* method presented in Sec. III E. In Fig. 8 the influence of fluid loading on the acoustic frequency response is analyzed. When computing the black line (FreeFEM without fluid loading) in Fig. 8 the fluid loading is neglected, but the added stiffness resulting from the closed cavity over which the membrane is inflated is taken into account. This added stiffness is of major importance, and can be accounted for even without a fully coupled finite element code [see Eq. (15)]. The red line (FreeFEM with fluid loading) is computed by taking into account both interior and exterior acoustic fluids. The uncoupled model provides a poor estimation of the radiated pressure. The frequencies and the amplitudes of the dominating modes are overestimated. When the fluid coupling is taken into account, the match of the resonance frequencies is much better, and the peak amplitudes also fit better. What is more, the three anti-resonances and resonances around 1490, 2880, and 4000 Hz, which correspond to standing waves in the cavity are well described by the coupled model.

D. Directivity of the dielectric elastomer loudspeaker

The radiated pressure is also measured on a circle of 1 m radius around the loudspeaker to investigate directivity effects. The measured and computed directivity at different frequencies are plotted in Fig. 9.

The model captures reasonably well the directivity of the prototype up to 4 kHz. At higher frequencies, the radiation is no longer axi-symmetric, due to imperfections of the prototype. This explains the differences observed between the measurements and the model. The radiation is omnidirectional up to approximately 3 kHz, when the loudspeaker is acoustically compact. Above that frequency, lobes can be observed, certainly due to casing effects. The result differs

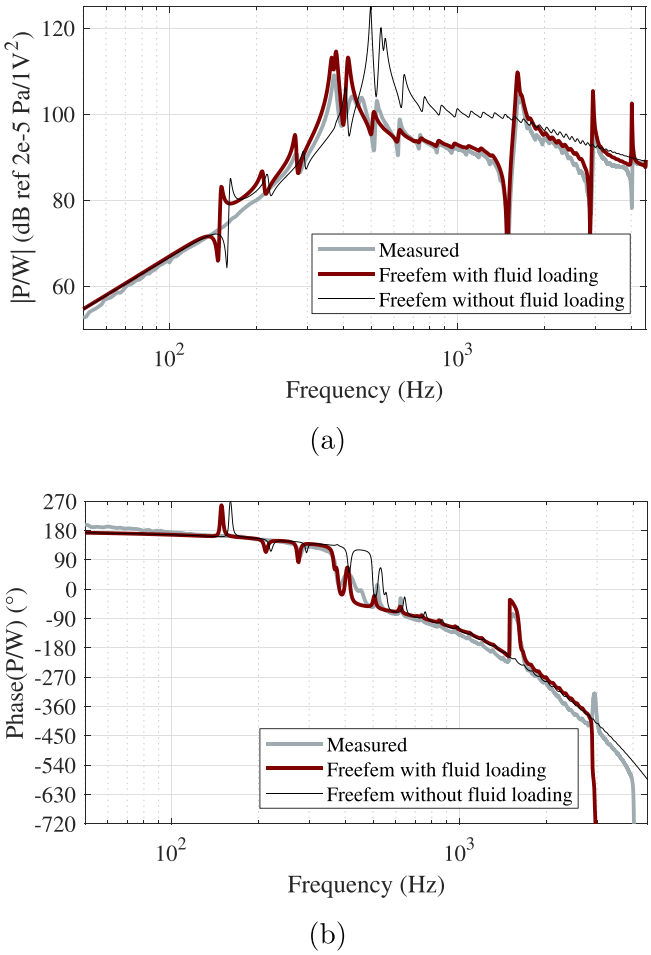

FIG. 8. (Color online) Frequency response function between the radiated pressure on axis at 12 cm, and the excitation signal W. (a) Amplitude. (b) Phase.

from the omnidirectional behavior up to 16 kHz observed by Hosoya *et al.*[4] However, their prototype was slightly smaller (3 cm), and was placed on an infinite baffle.

V. CONCLUSION

In this paper a multiphysics model of a dielectric elastomer membrane inflated over a closed cavity was presented.

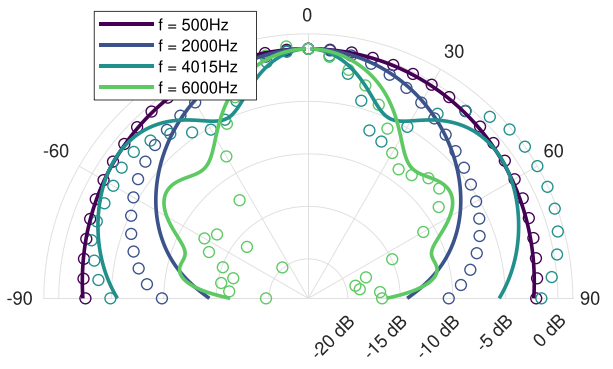

FIG. 9. (Color online) Directivity of the loudspeaker, at a distance of 1 m. The circles are measurements, and the solid lines calculations. The amplitude is normalized by the on-axis value.

Electro-mechanical coupling, non-linear elasticity, interior acoustics, and acoustic radiation in an open domain are taken into account. The model has been compared to experiments in a case where the membrane is used as a loudspeaker, and the radiated sound is well predicted.

This study also demonstrates the use of coupled fluid/structure resonance modes to compute the radiated acoustic pressure. This method appears to be easy to implement, as only a linear eigenvalue problem needs to be solved, and provides a large model order reduction. It is particularly efficient when several frequency responses of the same system but with different excitation forces are computed. The gain in computation speed would be useful for running optimization algorithms aiming at improving the behavior of the loudspeaker. The shape of the electrodes, the membrane thickness, the inflation pressure, the back cavity volume can now be optimized to improve various acoustic characteristics like flatness of the frequency response, directivity, low frequency cutoff, etc.

ACKNOWLEDGMENTS

The authors acknowledge the support of the French National Research Agency within the project SMArT (ANR-15-CE08-0007-02). This work has also benefited from the financial support of the LabeX LaSIPS (ANR-10-LABX-0040-LaSIPS) managed by the French National Research Agency under the "Investissements d'avenir" program (n^{o}ANR-11-IDEX-0003-02). The authors thank Marc Bonnet, Eliane Bécache, and Claude Stolz for fruitful comments and discussions.

[1]R. Pelrine, R. Kornbluh, Q. Pei, and J. Joseph, "High-speed electrically actuated elastomers with strain greater than 100%," Science **287**(5454), 836–839 (2000).
[2]See supplementary material at http://dx.doi.org/10.1121/10.0000930 for the implementation of axisymmetric PMLs in FreeFEM.
[3]R. Heydt, R. Pelrine, J. Joseph, J. Eckerle, and R. Kornbluh, "Acoustical performance of an electrostrictive polymer film loudspeaker," J. Acoust. Soc. Am. **107**(2), 833–839 (2000).
[4]N. Hosoya, S. Baba, and S. Maeda, "Hemispherical breathing mode speaker using a dielectric elastomer actuator," J. Acoust. Soc. Am. **138**(4), EL424–EL428 (2015).
[5]N. Hosoya, H. Masuda, and S. Maeda, "Balloon dielectric elastomer actuator speaker," Appl. Acoust. **148**, 238–245 (2019).
[6]E. Garnell, C. Rouby, and O. Doaré, "Dynamics and sound radiation of a dielectric elastomer membrane," J. Sound Vib. **459**, 114836 (2019).
[7]T. Sugimoto, A. Ando, K. Ono, Y. Morita, K. Hosoda, D. Ishii, and K. Nakamura, "A lightweight push-pull acoustic transducer composed of a pair of dielectric elastomer films," J. Acoust. Am. **134**(5), EL432–EL437 (2013).
[8]T. Sugimoto, K. Ono, A. Ando, Y. Morita, K. Hosoda, and D. Ishii, "Semicylindrical acoustic transducer from a dielectric elastomer film with compliant electrodes," J. Acoust. Soc. Am. **130**(2), 744–752 (2011).
[9]R. Heydt, R. Kornbluh, R. Pelrine, and V. Mason, "Design and performance of an electrostrictive polymer-film acoustic actuator," J. Sound Vib. **215**(2), 297–311 (1998).
[10]J. W. Fox and N. C. Goulbourne, "On the dynamic electromechanical loading of dielectric elastomer membranes," J. Mech. Phys. Solids **56**(8), 2669–2686 (2008).
[11]J. W. Fox and N. C. Goulbourne, "Electric field-induced surface transformations and experimental dynamic characteristics of dielectric elastomer membranes," J. Mech. Phys. Solids **57**(8), 1417–1435 (2009).
[12]J. Zhu, S. Cai, and Z. Suo, "Resonant behavior of a membrane of a dielectric elastomer," Int. J. Solids Structures **47**(24), 3254–3262 (2010).
[13]P. Filippi, D. Habault, P.-O. Mattei, and C. Maury, "The role of the resonance modes in the response of a fluid-loaded structure," J. Sound Vib. **239**(4), 639–663 (2001).
[14]S. Marburg, "Normal modes in external acoustics. Part I: Investigation of the one-dimensional duct problem," Acta Acust. Acust. **91**, 17 (2005).
[15]P. Lalanne, W. Yan, K. Vynck, C. Sauvan, and J.-P. Hugonin, "Light interaction with photonic and plasmonic resonances," Laser Photonics Rev. **12**(5), 1700113 (2018).
[16]W. Yan, R. Faggiani, and P. Lalanne, "Rigorous modal analysis of plasmonic nanoresonators," Phys. Rev. B **97**(20), 205422 (2018).
[17]J. Edmiston and D. Steigmann, "Analysis of nonlinear electrostatic membranes," in *Mechanics and Electrodynamics of Magneto- and Electro-Elastic Materials*, CISM International Centre for Mechanical Sciences (Springer, Vienna, 2011), pp. 153–180.
[18]A. N. Gent, "A new constitutive relation for rubber," Rubber Chem. Technol. **69**(1), 59–61 (1996).
[19]F. Carpi, I. Anderson, S. Bauer, G. Frediani, G. Gallone, M. Gei, C. Graaf, C. Jean-Mistral, W. Kaal, G. Kofod, M. Kollosche, R. Kornbluh, B. Lassen, M. Matysek, S. Michel, S. Nowak, B. O'Brien, Q. Pei, R. Pelrine, B. Rechenbach, S. Rosset, and H. Shea, "Standards for dielectric elastomer transducers," Smart Mater. Struct. **24**(10), 105025 (2015).
[20]X. Zhao, S. J. A. Koh, and Z. Suo, "Nonequilibrium thermodynamics of dielectric elastomers," Int. J. Appl. Mech. **03**(02), 203–217 (2011).
[21]A. Libai and J. G. Simmonds, *The Nonlinear Theory of Elastic Shells* (Cambridge University press, Cambridge, UK, 2005).
[22]H. J.-P. Morand and R. Ohayon, *Fluid Structure Interaction-Applied Numerical Methods* (Wiley, New York, 1995).
[23]J.-P. Berenger, "A perfectly matched layer for the absorption of electromagnetic waves," J. Comput. Phys. **114**(2), 185–200 (1994).
[24]F. Collino and P. Monk, "The perfectly matched layer in curvilinear coordinates," SIAM J. Sci. Comput. **19**(6), 2061–2090 (1998).
[25]F. Hecht, "New development in freefem++," J. Numer. Math. **20**(3-4), 251–266 (2013).